JIPB Journal of Integrative Plant Biology

Profiling of circular RNA N^6-methyladenosine in moso bamboo (*Phyllostachys edulis*) using nanopore-based direct RNA sequencing

Yongsheng Wang[1†], Huihui Wang[2†], Feihu Xi[1], Huiyuan Wang[2], Ximei Han[3], Wentao Wei[2], Hangxiao Zhang[2], Qianyue Zhang[3], Yushan Zheng[3], Qiang Zhu[2], Markus V. Kohnen[2], Anireddy S. N. Reddy[4] and Lianfeng Gu[2]*

1. Basic Forestry and Proteomics Research Center, College of life science, Fujian Agriculture and Forestry University, Fuzhou 350002, China
2. Basic Forestry and Proteomics Research Center, College of Forestry, Fujian Agriculture and Forestry University, Fuzhou 350002, China
3. College of Forestry, Fujian Agriculture and Forestry University, Fuzhou 350002, China
4. Department of Biology and Program in Cell and Molecular Biology, Colorado State University, Fort Collins, Colorado, USA
†These authors contributed equally to this work.
*Correspondence: Lianfeng Gu (lfgu@fafu.edu.cn)
doi: 10.1111/jipb.13002

New Technology

Abstract N^6-methyladenosine (m^6A) is a prevalent modification in messenger RNAs and circular RNAs that play important roles in regulating various aspects of RNA metabolism. However, the occurrence of the m^6A modification in plant circular RNAs has not been reported. A widely used method to identify m^6A modifications relies on m^6A-specific antibodies followed by next-generation sequencing of precipitated RNAs (MeRIP-Seq). However, one limitation of MeRIP-Seq is that it does not provide the precise location of m^6A at single-nucleotide resolution. Although more recent sequencing techniques such as Nanopore-based direct RNA sequencing (DRS) can overcome such limitations, the technology does not allow sequencing of circular RNAs, as these molecules lack a poly(A) tail. Here, we developed a novel method to detect the precise location of m^6A modifications in circular RNAs using Nanopore DRS. We first enriched our samples for circular RNAs, which we then fragmented and sequenced on the Nanopore platform with a customized protocol. Using this method, we identified 470 unique circular RNAs from DRS reads based on the back-spliced junction region. Among exonic circular RNAs, about 10% contained m^6A sites, which mainly occurred around acceptor and donor splice sites. This study demonstrates the utility of our antibody-independent method in identifying total and methylated circular RNAs using Nanopore DRS. This method has the additional advantage of providing the exact location of m^6A sites at single-base resolution in circular RNAs or linear transcripts from non-coding RNA without poly(A) tails.

Edited by: Binglian Zheng, Fudan University, China
Received Jun. 13, 2020; **Accepted** Jul. 29, 2020; **Online on** Jul. 31, 2020

INTRODUCTION

Although circular RNAs (circRNA) were discovered over 40 years ago, for much of this time they were mainly considered to be aberrant by-products of the splicing reaction (Nigro et al. 1991; Cocquerelle et al. 1992; Capel et al. 1993; Cocquerelle et al. 1993; Pasman et al. 1996). With the development of circRNA-enriched RNA sequencing techniques and circRNA-specific bioinformatics tools, it became clear that circRNAs can be generated from coding genes by back-splicing in diverse eukaryotes, including fungi, protists, plants, worms, fish, insects, and mammals (Jeck et al. 2013; Salzman et al. 2013; Westholm et al. 2014; Wang et al. 2014a; Ivanov et al. 2015). Recently, circRNAs were shown to regulate various biological processes in plants and animals such as binding to miRNAs, interaction with RNA-binding proteins, and the regulation of transcription, splicing of parental genes, and translation. Stable circRNAs function as miRNA sponges that compete with miRNA binding sites (Ebert et al. 2007; Franco-Zorrilla et al. 2007;

Poliseno et al. 2010). A striking example in the mammalian brain is a highly conserved circRNA (*Cerebellar Degeneration-Related protein 1* antisense, or CDR1as), which contains over 60 binding sites for the microRNA miR-7 (Hansen et al. 2011, 2013; Memczak et al. 2013). Nuclear-retained circRNAs modulate the transcription of their precursor transcripts (Zhang et al. 2013; Li et al. 2015; Conn et al. 2017a)

In addition to their role as regulators of transcription, circRNAs also regulate the alternative splicing of their parental transcripts. For example, CircSEP3 derived from the *Arabidopsis* (*Arabidopsis thaliana*) *SEPALLATA3* (*SEP3*) locus, enhances exon skipping in *SEP3* pre-mRNA (Conn et al. 2017b). Exonic circRNAs also interact with RNA-binding proteins and influence their function. For instance, circANRIL (circular antisense non-coding RNA in the *INK4* locus) can bind to the essential 60S-preribosomal assembly factor peccadillo homolog 1 (PES1) to inhibit ribosome biogenesis in vascular smooth muscle cells and macrophages (Burd et al. 2010; Holdt et al. 2016). Currently, RNase R enrichment of circRNAs followed by high-throughput sequencing to generate short reads is the gold standard to detect circRNAs (Li et al. 2016b; Zhang et al. 2019a). However, identification of circRNAs using single-molecule long-read methods such as Nanopore direct RNA sequencing (DRS), which offer several advantages in detecting RNA modifications, has never been reported (Parker et al. 2020).

In addition to the emerging functions of circRNA in epigenetics, RNA modifications are attracting widespread attention as another type of epigenetic regulation. Among all known RNA modifications, N^6-methyladenosine (m^6A) is the best-characterized and the most abundant in eukaryotes (Wei et al. 1975; Li and Mason 2014). This modification occurs on RNA co-transcriptionally by a writer complex consisting of METHYLTRANSFERASE-LIKE 3 (METTL3), METTL14, and Wilms tumor 1-associating protein (WTAP) (Wei et al. 1975; Bokar et al. 1997; Liu et al. 2014; Ping et al. 2014; Wang et al. 2014b), and is removed by the m^6A erasers fat mass and obesity-associated protein (FTO) or alkylated DNA repair protein AlkB homolog 5 (ALKBH5) (Jia et al. 2011; Zheng et al. 2013). m^6A-containing RNAs are recognized by reader proteins using different mechanisms that involve YTH-domain-containing proteins (YTHDF1-3, YTHDC1-2) (Wang et al. 2015; Shi et al. 2017), heterogeneous Nuclear Ribonucleoproteins (HNRNPC/G, HNRNPA2B1) (Alarcon et al. 2015; Liu et al. 2015, 2017; Wu et al. 2018), insulin-like growth factor two mRNA-binding proteins 1-3 (IGF2BP1-3) (Huang et al. 2018), and fragile X mental retardation 1 (FMR1) (Edupuganti et al. 2017; Zhang et al. 2018a).

Recent studies have revealed that m^6A RNA methylation affects multiple aspects of mRNA metabolism, including mRNA localization, stability, polyadenylation, and translation (Meyer and Jaffrey 2014; Yue et al. 2015). The m^6A eraser ALKBH5 and the m^6A reader YTHDC1 participate in m^6A regulation, affecting the export of mRNAs from the nucleus to the cytoplasm (Zheng et al. 2013; Roundtree et al. 2017). The upregulation of m^6A levels in pre-mRNAs leads to more alternative polyadenylation (APA) in cultured cells (Ke et al. 2015; Molinie et al. 2016). Furthermore, the m^6A reader YTHDC2 enhances the cap-independent translation efficiency of target mRNAs (Hsu et al. 2017; Wojtas et al. 2017; Jain et al. 2018) through the YTHDF2 protection mechanism, whereas the cytosolic proteins YTHDF3 and YTHDF1 interact with ribosomal proteins to promote mRNA translation (Bailey et al. 2017; Li et al. 2017; Shi et al. 2017). Interestingly, m^6A modifications are prevalent in circRNAs and play a key role in splicing and translational regulation (Yang et al. 2017; Tang et al. 2020). It is worth noting that the fruit fly (*Drosophila melanogaster*) circMbl (a circRNA from the *Muscleblind* (*Mbl*) locus) and the human (*Homo sapiens*) circZNF609 (a circRNA from Zinc Finger Protein 609) can be translated in a cap-independent manner because they contain internal ribosome entry sites (IRES) and use the same start codon as their parental mRNAs (Legnini et al. 2017; Pamudurti et al. 2017). The translation of circular RNAs may be regulated by m^6A modifications (Legnini et al. 2017; Pamudurti et al. 2017; Yang et al. 2017).

The m^6A modification preferentially occurs in the consensus RNA motif RRACH (R = G or A; H = A, C or U) based on high-throughput sequencing data (Csepany et al. 1990; Harper et al. 1990). Currently, m^6A modifications in linear transcripts are detected mainly by antibody-based immunoprecipitation methods (Dominissini et al. 2012, 2016; Meyer et al. 2012; Arango et al. 2018) and digestion of mRNAs by the m^6A-sensitive bacterial RNase MazF (MAZTER-seq) (Garcia-Campos et al. 2019; Zhang et al. 2019b). The recent emergence of

DRS techniques based on Oxford Nanopore Technologies (ONT) provides a new way to detect the underlying modifications in linear transcripts at single-nucleotide resolution (Liu et al. 2019). Unlike linear RNA, circular RNAs have a covalent closed-loop structure without a 3′ poly(A) tail (Lasda and Parker 2014; Chen 2016; Wilusz 2018), which is required for DRS on the ONT platform. Thus, the current strategy for ONT-type library preparation and the associated computational pipeline cannot currently be used to identify m^6A-marked circRNAs. CircRNAs in animals are m^6A-modified and have the potential to initiate cap-independent translation (Yang et al. 2017). Thus, there is a crucial need to detect m^6A-marked circular RNAs at single-base resolution using direct RNA sequencing so as to explore their translatability.

Moso bamboo (*Phyllostachys edulis*), for which a chromosome-level reference genome is available, is a large woody bamboo with high ecological, economic, and cultural value in China (Zhao et al. 2018a). In addition, moso bamboo presents striking characteristics, such as late flowering (Ge et al. 2017) and fast growth rate (Li et al. 2016a), which contributes to its economic value in delivering plant biomass in a short period. Phytohormone-mediated signaling largely contributes to growth regulation in bamboo culms (Peng et al. 2013); in particular, gibberellic acid (GA) participates in moso bamboo stem elongation (Zhang et al. 2018b; Shou et al. 2020). We have previously shown that circular RNAs are involved in the rapid growth exhibited by moso bamboo and that they modulate the levels of linear transcripts derived from their parental genes (Wang et al. 2019). However, whether such circRNAs might be modified by m^6A in response to GA treatment has not been reported in moso bamboo or other plants.

Here, we developed a novel method to detect m^6A-marked circular RNAs in moso bamboo through direct RNA sequencing using ONT at single-nucleotide resolution. This method involves enriching for circRNAs using a three-step protocol. The circRNAs are then fragmented and used for direct RNA sequencing with a customized reverse transcription adapter. To analyze the RNA reads and identify circRNAs and m^6A modifications, we developed a new computational pipeline. Our analysis identified 470 circRNAs in moso bamboo, of which about 10% of exonic circRNAs contained m^6A modifications. In summary, we developed a new method to identify total and methylated circRNAs using direct RNA sequencing by ONT. This study expands the diversity of methods available for detecting circRNAs, pinpoints the precise location of m^6A modifications, and paves the way for a thorough investigation of the dynamics and cellular functions of m^6A methylated circRNAs.

RESULTS

Library preparation for direct sequencing of circRNAs

To enrich highly pure circular RNAs in total RNA, we developed a novel procedure for DRS of circular transcripts (Figure 1A). We extracted total RNA from 4-week-old bamboo seedlings treated with GA_3 and visualized the RNA by agarose gel electrophoresis (Figure 1B). Considering the small fraction of circular RNAs and the high amount of input RNA required for Nanopore DRS, we digested 100 μg of total RNA with RNase R, an almost 25-fold excess compared to the amount used in the RPAD method (Panda et al. 2017). Circular RNAs, such as PH02Gene34473 (which we used as a marker), were enriched after RNase R digestion (Figure 1C). However, linear transcripts for *ACTIN* were not completely depleted, suggesting that a simple RNase R treatment would not completely digest linear RNAs for highly expressed housekeeping genes, in agreement with previous reports (Panda et al. 2017).

To further remove non-circular RNAs, we artificially ligated poly(A) tails to residual contaminating linear RNAs with and without secondary structures, and then depleted them from our samples using oligo $(dT)_{25}$ beads. After this purification step, RT-PCR analysis demonstrated that linear RNAs (such as PH02Gene34082) were eliminated, whereas circular RNAs (such as PH02Gene34473) were strongly enriched (Figure 1D). After removing residual rRNAs with ribodepletion probes, we obtained highly pure circRNAs. We then fragmented and dephosphorylated circular RNAs, followed by purification (Figure 1A). Next, we synthesized the first complementary DNA (cDNA) strand from our purified linear RNA fragments by attaching a customized RT adapter including ten degenerate primers 'N' (N = A/C/G/T) to replace the usual oligo$(dT)_{10}$ used for Nanopore DRS. Finally, we ligated a sequencing adapter to the generated cDNAs

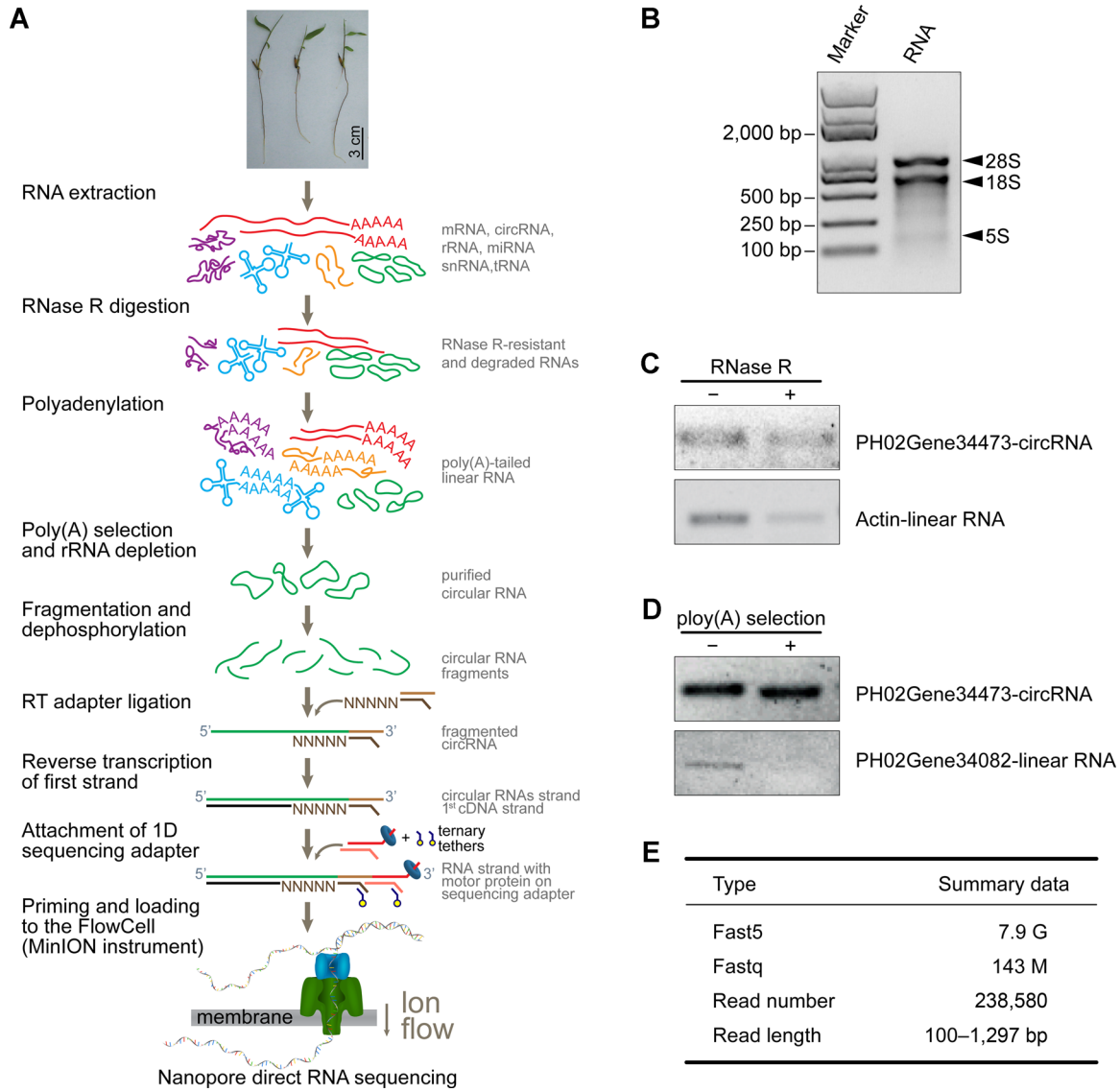

E

Type	Summary data
Fast5	7.9 G
Fastq	143 M
Read number	238,580
Read length	100–1,297 bp

Figure 1. Circular RNA library preparation and experimental validation of circular RNAs enrichment

(**A**) Schematic diagram of circular RNA library preparation for Nanopore direct RNA sequencing. Total RNA was extracted from bamboo seedlings treated with GA. Circular RNAs were then enriched by RNase R digestion, polyadenylation, poly(A) selection and rRNA depletion. Subsequently, circular RNAs were fragmented, dephosphorylated, ligated to a modified RT adapter, reverse transcribed. Finally, a sequencing adapter (red lines) was added and the final products were sequenced on the MinION platform. (**B**) Agarose gel electrophoresis of total RNA. (**C**) Validation of RNase R digestion using a known circRNA (PH02Gene34473-circRNA) and linear RNA (actin-linear RNA) as negative and positive controls, respectively. (**D**) Validation of removal of poly(A)-tailed RNAs using circRNA (PH02Gene34473-circRNA) and linear RNA (PH02Gene34082-linear RNA) as positive and negative controls, respectively. (**E**) Summary of generated Nanopore DRS reads (fast5 and fastq).

and subjected them to direct RNA sequencing on a MinION Nanopore sequencer (Figure 1A).

It should be noted that the motor protein was linked to the RNA strand, so that the RNA was sequenced to detect RNA modification, and not the first-strand cDNA, which was merely present to reduce or eliminate RNA secondary structures to ensure efficient RNA strand translocation through the Nanopore (Soneson et al. 2019). Overall, we obtained raw fast5 file (7.9 Gbite in size), corresponding to 143 million reads (fastq file) after base calling, including 238,580 reads (Figure 1E) with a sequence length ranging from 100 to 1,297 nt.

Identification of circular RNAs generated from Nanopore DRS data

There is currently no available computational pipeline to identify circular RNAs produced from DRS reads. To map single-molecule sequencing reads, including back-splicing junction sites, we developed a *de novo* computational pipeline for identifying circRNAs from DRS reads, which is based on back-splicing across splice junctions (i.e., covalent joining between a downstream splice donor site and an upstream acceptor splice site), a special characteristic of circRNAs (Zhang et al. 2014). Briefly, we joined all exons or introns from gene annotations by simulating back-splicing to construct a virtual library of circRNA sequences (Figure 2A), and then aligned all reads generated from DRS to this virtual library using the minimap2 algorithm (Li 2016). We selected reads spanning back-splicing junctions as potential circRNAs. In total, this *de novo* strategy allowed us to identify 428 exonic circular RNAs (circRNAs) and 42 intronic circular RNAs (ciRNAs), respectively (Figure 2B, Table S1). To further confirm these circular RNAs from Nanopore DRS, we selected four candidates to validate their circularity by RNase R digestion, followed by RT-PCR. All candidates showed a PCR product of the expected size even after RNase R treatment, in contrast to the linear RNA control (Figure 2C).

Most detected exonic circular RNAs appeared to be processed from multiple exons, most commonly two or three, although circRNAs with only one circularized exon accounted for 5.9% of the circularized exons (Figure 2D, left panel). Overall, the length of back-spliced junction reads was much longer than that of all reads, which included both reads with back-splicing junction and fragmented reads without back-splicing junction from Nanopore sequencing (Figure 2D, right panel). The length of single circularized exons was much longer than that of multiple circularized exons (Figure 2E, right panel), which is consistent with a previous report indicating that biogenesis of circularized exons may prefer a given minimal length to maximize exon(s) circularization (Zhang et al. 2014). We next asked whether these identified circRNAs were associated with specific processes or functions. We performed a Gene Ontology overrepresentation test using the parental genes of these circRNAs. As shown in Figure 2F, our results suggest that parental genes are involved in specific processes, including chromosome organization and chromosome segregation. For example, we detected a circ-RFC1 originating from the gene PH02Gene11283, which encodes Replication Factor C subunit 1 (RFC1) and is required during meiosis for DNA double-strand break repair during meiotic homologous recombination (Liu et al. 2013).

Characterization of circular RNAs containing m^{6}A modification

To test for the existence of RNA modifications such as m^{6}A modification in circRNAs, we first statistically determined whether our list of candidate circRNAs contained the m^{6}A-modified consensus RRACH site. As indicated in Figure 3A and Table S2, approximately 99.2% of all identified circRNAs included potential RRACH motifs, a prerequisite for m^{6}A-modification. We then applied the EpiNano tool (Liu et al. 2019) to identify real m^{6}A-marked circRNAs from DRS reads. Overall, we identified m^{6}A modifications in 10.7% of our circRNAs.

Most m^{6}A modifications appeared to occur near donor or acceptor splice sites (Figure 3B), an observation that is consistent with a recent report (Tang et al. 2020) and indicates that m^{6}A modifications may regulate the back-splicing step. We further evaluated the features of circRNAs with or without m^{6}A modifications. Compared with non-m^{6}A circRNAs, m^{6}A circRNAs more commonly originated from three exons (Figure 3C), although exon length in m^{6}A circRNAs was comparable to that of non-m^{6}A circRNAs (Figure 3D). However, exons from linear transcripts with m^{6}A modifications showed a longer length than linear transcripts without m^{6}A modifications ($P = 2.2 \times 10^{-16}$), based on a typical Nanopore DRS library generated without the RNase R digestion step (Figure 3D). Furthermore, we noticed that the flanking introns of circRNAs containing m^{6}A modifications were much longer than those of circRNAs lacking m^{6}A modifications (Figure 3E). However, this difference in length could not be attributed to the presence of transposable elements within these long flanking introns.

A Gene Ontology (GO) enrichment analysis of the parental genes generating m^{6}A-marked circRNAs (Figure 3F–H) revealed a number of highly enriched biological processes, such as amyloplast organization and glutamine biosynthetic process. We also observed enrichment for the cellular components chloroplasts

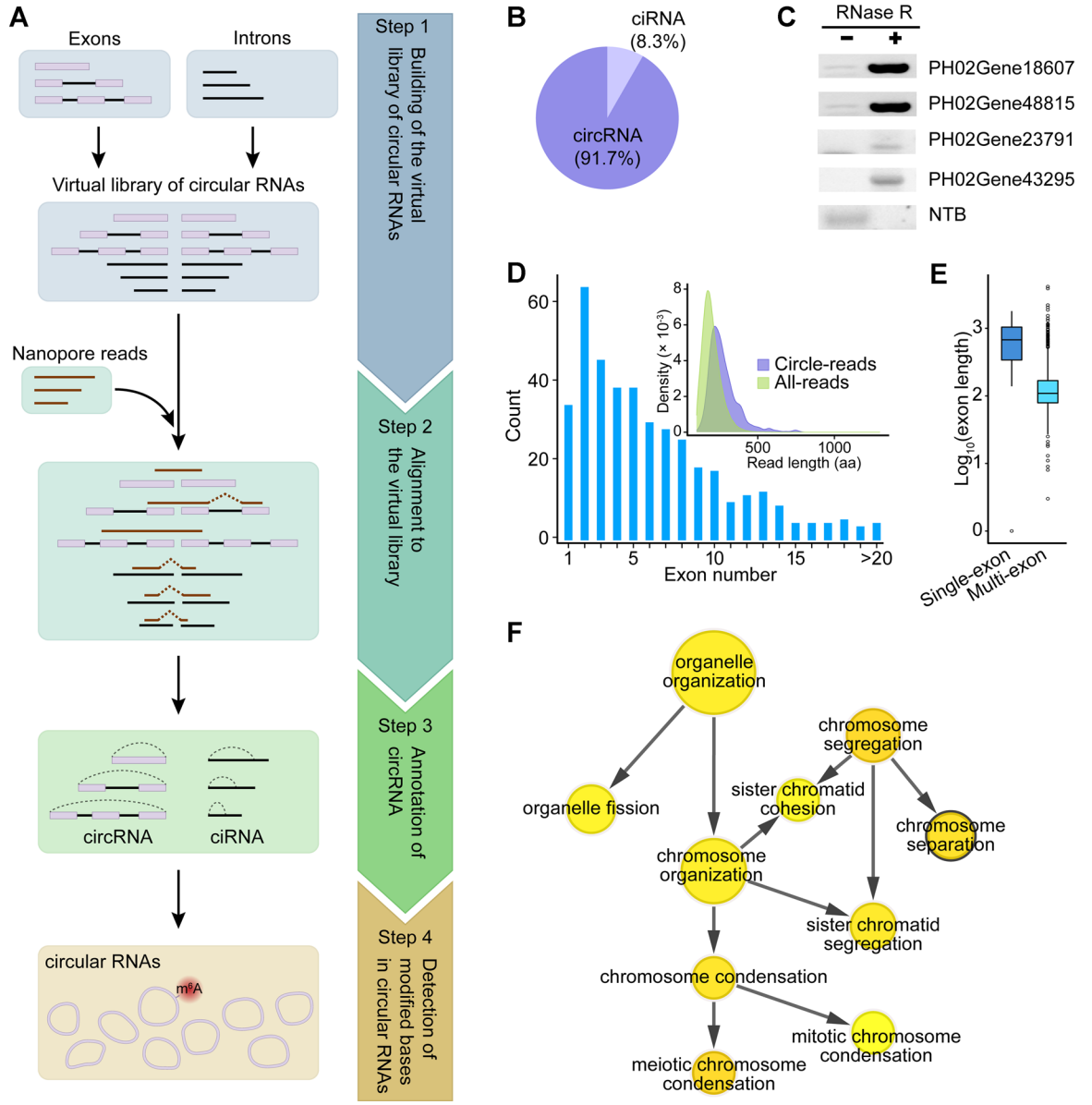

Figure 2. Identification and characterization of circular RNAs from Nanopore DRS

(**A**) Schematic diagram of the accurate detection and annotation of full-length circRNAs from Nanopore data. All annotated exons and introns were first used to construct a simulated library of back-splicing junctions (Step 1). Then, Nanopore reads (brown lines) were mapped to simulated back-splicing junctions using minimap2; the reads spanning back-splicing junctions were retained as circRNA candidates for downstream analysis (Step 2). These candidates were compared to the predicted circRNAs with a customized algorithm using known gene annotations (Step 3). The m^6A modifications in circRNAs were detected using EpiNano software (Step 4). ciRNAs: intronic circular RNAs. (**B**) The number of all circRNAs. (**C**) RT-PCR validation of circular RNAs with divergent primers resistance to RNase R treatment. Total RNA from seedlings with (+) or without (-) RNase R treatment. Linear RNAs NTB was control. (**D**) Number of circularized exons (left panel) and length distribution (right panel) of back-spliced reads for all circRNAs. (**E**) Length of circularized exons. (**F**) GO enrichment analysis for circRNA parental genes.

and thylakoids, and phosphatase inhibitor activity and glycogen debranching enzyme activity were among enriched molecular functions associated with circRNA parental genes. For instance, five m^6A modifications were detected in circ-AtI-2 generated from gene PH02Gene48815 encoding a homolog to ARABIDOPSIS PROTEIN PHOSPHATASE INHIBITOR-2 (AtI-2), which may promote the interaction of TYPE ONE PROTEIN

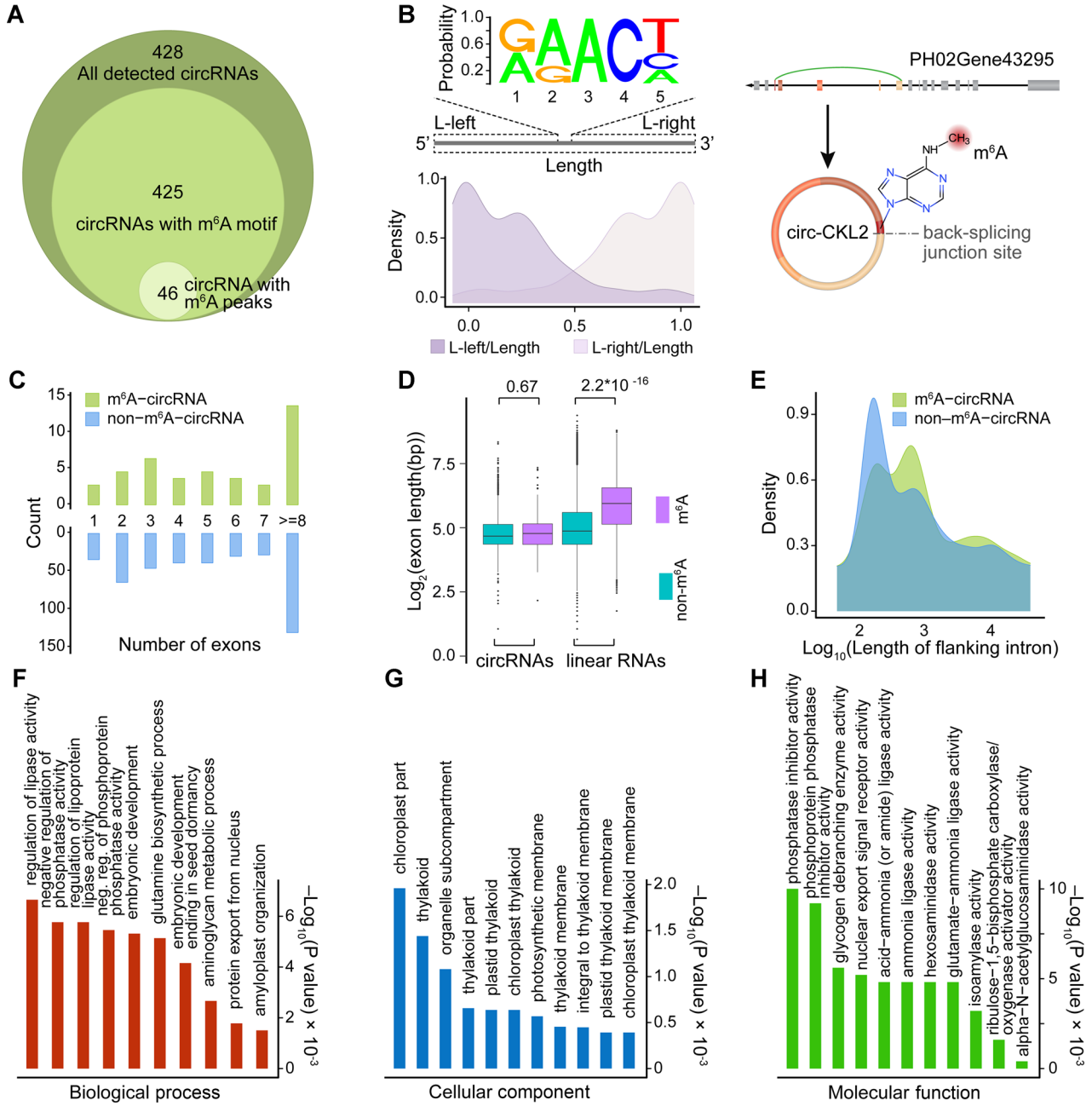

Figure 3. Characterization of circular RNAs containing the m^{6}A modification

(**A**) The number of circRNAs containing the m^{6}A modification. Outer circles indicate total detected circRNAs (428), the middle circle represents circRNAs with potential RRACH motifs (425) and the inner circle indicates circRNAs containing m^{6}A modification, supported by a signal in Nanopore DRS read (46). (**B**) Consensus m^{6}A motifs (RRACH) are enriched around back-splicing junction sites (left panel, Top). Density indicates the distance between RRACH motifs to 5′ back-splicing junction sites or 3′ back-splicing junction sites, respectively (left panel, Bottom). One example from PH02Gene43295 presents an m^{6}A site, which is close to the back-splicing junction (right panel). (**C**) Number and length distribution of circularized exon circRNAs with or without m^{6}A modifications. Most circRNAs with m^{6}A modification contain multiple back-spliced exons. (**D**) Box plots of the distribution of exon length (y axis) in circRNAs with or without m^{6}A modifications and linear transcripts as control. (**E**) Density plot showing that flanking introns of circRNAs with m^{6}A modifications are longer than those of circRNAs without m^{6}A modifications. (**F**–**H**) Gene Ontology (GO) functional enrichment analysis was performed for the parental genes of circRNAs with m^{6}A modifications.

PHOSPHATASE 1 (TOPP1) and the abscisic acid receptor PYRABACTIN-RESISTANCE1 (PYR1)-LIKE 11 (PYL11) (Templeton et al. 2011).

Translation of circRNAs

To determine the coding potential of circular transcripts identified by Nanopore DRS, we processed all single exon circRNAs and multiple exon circRNAs (excluding intron sequences) for coding potential through the classification tools Coding-Non-Coding Index (CNCI) and Coding Potential Calculator (CPC), as well as the Swiss-Port database. CNCI, CPC and Swiss-Port identified 331 circRNAs with translation potential, or 77.3% of all circRNAs (Figure 4A).

To determine if their translation might be promoted by internal ribosome entry sites (IRES), we screened circRNAs for the presence of IRES *cis*-regulatory elements using framed k-mer features with the IRESfinder tool. Of our initial set of 331 circRNAs with translation potential, 143 circRNAs had one IRES, accounting for 33.4% of all detected circRNAs (Figure 4B). In addition, circRNAs contained slightly more IRES *cis*-elements than the flanking exonic regions from the same host genes (Figure 4B). These results strongly indicate that circularized transcripts possess a similar coding potential as linear transcripts and that the translation potential of circRNAs may also rely on the presence of IRES *cis*-elements. Interestingly, circRNAs also originate from the m^{6}A effector loci *METTL14* (PH02Gene11019) and *YTHDF1-3* (PH02Gene28571), as noted in our previous study (Wang et al. 2019). At least in the case of *METTL14*, an IRES *cis*-element is present (PH02Gene11019) in the circRNA. However, more experimental evidence will be needed to determine whether circRNA derived from *METTL14* can be translated into a protein with biological function (Figure 4C).

We next undertook a systematic identification of all open reading frames (ORFs) encoded by our list of circRNAs. To this end, we multiplied the sequences of single exon circRNAs and multiple exons circRNAs (excluding intron sequences) four times to detect ORFs, only keeping non-redundant predicted ORFs for downstream analysis (Figure 4D). We obtained 237 ORFs from 150 circRNAs with predicted ORF lengths ranging from 200 to 1,000 aa (Figure 4E). The percentage of ORFs spanning the back-splicing junctions of circRNAs accounted for approximately 50% of all predicted ORFs (Figure 4E). Using this set of circRNA-encoded proteins, we performed BLAST homology searches to identify orthologues in other species. Of these 237 ORFs, we identified 135 ORFs, or 56.9%, with clear homologs with known functions (Figure 4F; Table S3). For example, peptides translated from the circRNA circ-KEL1, generated from the PH02Gene10106 locus, showed homology to the yeast (*Saccharomyces cerevisiae*) protein KEL1, a kelch-repeat-containing protein that is involved in cell morphogenesis and cell fusion by antagonizing the Protein Kinase C (PKC1) pathway (Figure 4G) (Ghaemmaghami et al. 2003). These observations imply that peptides generated from circRNAs may function as proteins and may therefore regulate biological pathways composed of proteins that are translated from linear molecules.

Translation of circRNAs lacking a 5′ cap or a poly (A) tail can still occur through IRES, or be driven by m^{6}A RNA modification, such as the circRNAs circ-ZNF609, circ-Mbl, and circ-FBXW7 (F-box/WD repeat-containing protein 7) (Legnini et al. 2017; Liang et al. 2017; Yang et al. 2018). Moreover, we identified 46 circRNAs containing m^{6}A modification, of which 11 can potentially be translated into long, continuous ORFs (Figure 4H). For example, circ-GAMYB (GA MYB domain protein) generated from PH02Gene34674 contained a m^{6}A modification in upstream 160 bp of the start codon of its predicted ORF. Taken together, this study suggests that translation of circularized transcripts might be driven by IRES or m^{6}A modifications.

DISCUSSION

Circular RNAs (circRNAs), formed by back-splicing known as non-canonical 3′ to 5′ end-joining event, are widely present and conserved across eukaryotic organisms (Zhang et al. 2014). Previous studies have shown that circRNAs may function as miRNA sponges or modulate gene expression at both the transcriptional and splicing levels (Zhang et al. 2013; Li et al. 2015; Chuang et al. 2018). More recently, several studies pointed out that m^{6}A can promote the translation of circRNAs and that m^{6}A modification of circRNAs is written and read by the same machinery (METTL3/14 and YT521-B Homology (YTH) proteins) used for mRNAs, although often at different locations (Yang et al. 2017). Current technologies for detecting RNA modifications

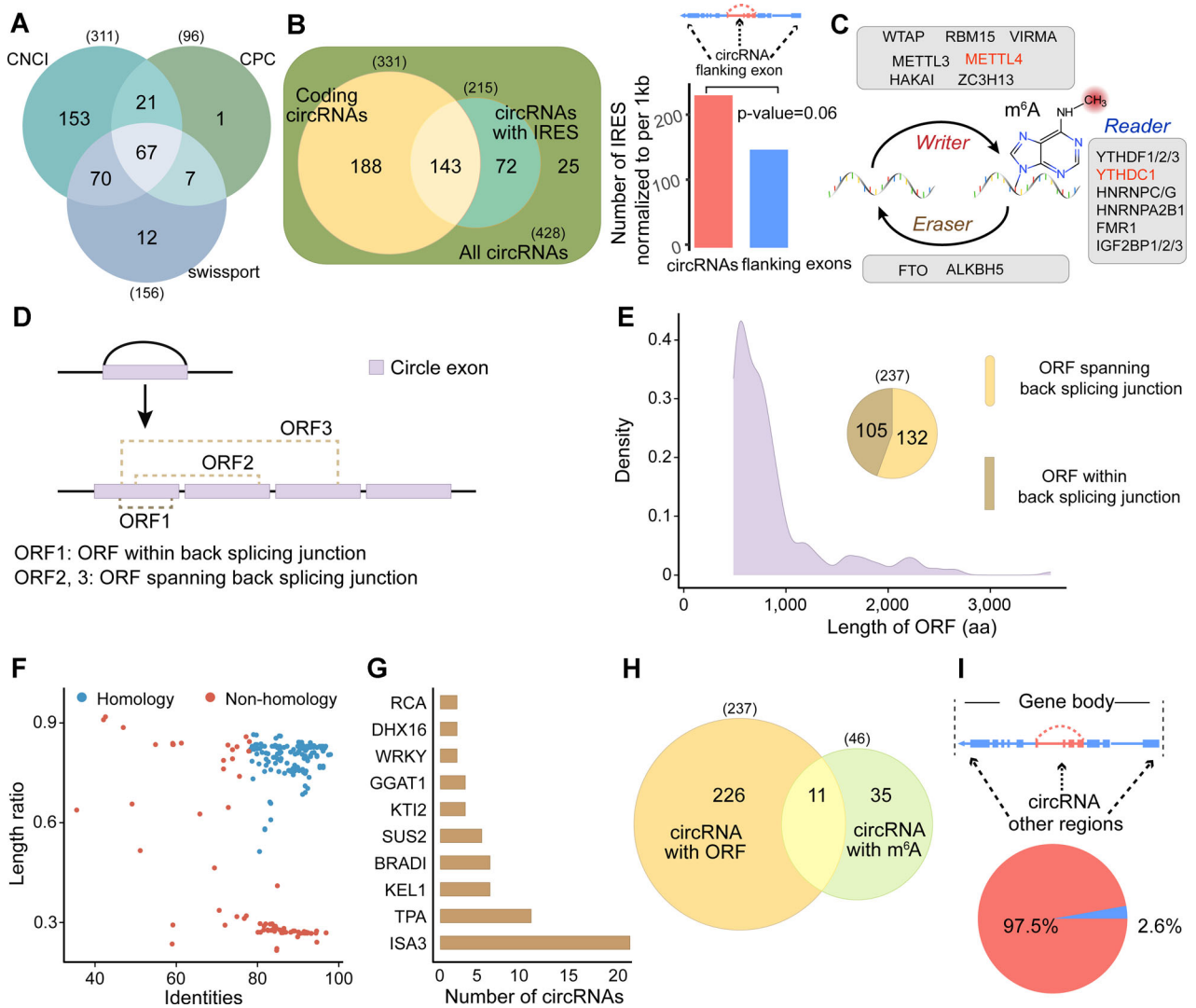

Figure 4. Translation of circRNAs

(**A**) The number of potential protein-coding circRNAs. Circles with different colors indicate potential protein-coding circRNAs supported by Coding-Non-Coding Index (CNCI), Coding Potential Calculator (CPC), and Swiss-Port. (**B**) Left panel presented the number of circRNAs containing internal ribosome entry sites (IRESs). Right panel presented the number of IRES (Normalized to 1 kb) in circRNA regions and flanking exons regions in their host gene. (**C**) Summary of the m^{6}A modification machinery, including writers, erasers and readers that may regulate methylation of circular RNAs. Red indicates the m^{6}A methyltransferase complex that might generate methylated circRNAs. (**D**) Schematic diagram for identifying ORFs in circRNAs. Each circRNA sequence, excluding intron sequences, were joined four times for ORFs prediction. (**E**) Density plot indicates the length of predicted ORFs. Pie chart shows that approximately 50% of predicted ORFs spanned circRNA junctions. (**F**) Homology-based annotation for predicted ORFs. 135 ORFs originating from 65 circRNAs shared significant homology with known proteins. (**G**) Bar plot indicates the top 10 known proteins that showed homology to the above-mentioned ORFs. (**H**) Venn diagram showing the overlap between ORF-containing circRNAs and circRNAs with m^{6}A modifications. (**I**) Distribution of reads generated from DRS in the body of an annotated gene. Red and blue indicate the percentage of reads in the circRNA regions, or flanking regions of host gene, respectively.

that use antibody immunoprecipitation (Dominissini et al. 2012, 2016; Meyer et al. 2012; Carlile et al. 2014; Schwartz et al. 2014; Arango et al. 2018) cannot identify the underlying modified sites in circRNAs at single-nucleotide resolution. Although Nanopore-based DRS techniques can detect modifications from linear RNAs (Garalde et al. 2018; Liu et al. 2019), they are limited to linear transcripts with poly(A) tails. Furthermore,

the lack of an adequate computational pipeline has restricted the identification of RNA modifications in circRNAs from DRS data.

To overcome these limitations, we improved on the library construction approach of ONT DRS to identify any transcript, with or without a poly(A) tail. In parallel, we developed a *de novo* computational pipeline to detect circular transcripts and RNA modifications in native circRNA sequences that do not contain a poly(A) tail. Using the method described here, we identified 428 circRNAs (exonic circular RNAs) and 42 ciRNAs (intronic circular RNAs). The intrinsic features of circRNAs characterized in this study, such as distribution of exon numbers and length, were consistent with previous reports (Zhang et al. 2014), which validated the reliability of our approach from DRS. This study also demonstrates that ONT DRS can efficiently detect native circular transcripts and identify RNA modifications within circRNAs, which had not been reported for circRNAs in either plants or animals with this technology. However, Nanopore-based DRS using a MinION device produced a lower depth of coverage than next-generation sequencing on an Illumina platform, a clear limitation for the application of Nanopore DRS to the quantification of native circular transcripts and their m^6A modifications. With improvements in sequencing depth for ONT using the GridION and PromethION systems, the method described in this study may become applicable to obtaining quantitative information on circRNAs and RNA modifications.

In this study, we modified the RPAD method (Panda et al. 2017) to enrich for circular RNA (Figure 1A). Our method significantly enriched reads from circRNA regions (97.5%) relative to other regions of the host genes (2.6%) (Figure 4I), suggesting that the RPAD method almost completely removed all linear mRNA fragments from the same parental genes, greatly decreasing background noise during downstream analysis. However, circRNAs expressed at low levels might be under-represented by this method due to the multiple filtering during library construction.

The advantage of the ONT platform is that it allows the identification of RNA modifications in individual native circular RNA sequences at single-nucleotide resolution. In this study, we detected 99 m^6A modified sites in only GA-treated seedlings. While our method allowed the identification of individual circRNA molecules and the detection of m^6A modification on individual circRNAs, it cannot currently provide an accurate quantification of m^6A modifications at a transcript-based level, which would open up the quantitative profiling of m^6A abundance using Nanopore DRS between any two conditions or genotypes. We hope to reveal differential m^6A-modified circRNAs sites in response to phytohormone treatment in moso bamboo, when the methods for quantifying m^6A sites become available for Nanopore DRS. In addition to m^6A modifications, other RNA modifications such as m^1A and m^5C from individual circRNA molecules might also become accessible to detection. However, a corresponding computer algorithm would have to be developed to accommodate multiple RNA modifications. Currently, only computational pipeline for the detection of the m^6A identification has been reported.

The coding potential of the circular transcripts identified in our study by the ONT platform is strongly supported by multiple lines of evidence. For example, 33.4% of all detected circRNAs possessed IRES *cis*-elements. In addition, 56.9% of all ORFs generated from circRNAs may have similar functions to proteins they show strong homology for in other organisms. Here, due to the low depth of MinION sequencing, we did not provide the distribution of m^6A modifications near the start/stop codons, which might be associated with protein-coding potential. Thus, further research is essential to uncover how these m^6A modifications affect the translation of circular molecules using GridION or PromethION systems, which can provide higher depth of coverage to quantify circular RNAs and RNA modifications.

MATERIALS AND METHODS

Plant materials and RNA extraction

We collected 4-week-old whole moso bamboo (*Phyllostachys edulis*) seedlings grown on Murashige and Skoog (MS) medium and in long-day conditions (16 h light/8 h dark) after being treated with gibberellic acid (GA_3, 100 μM) for 4 h. The seedlings were immediately frozen in liquid nitrogen and stored at –80°C prior to total RNA extraction. Total RNAs were isolated with the RNAprep Pure Plant Kit (Cat. #DP441, Tiangen). RNA quality was assessed by agarose gel electrophoresis and

measurements on a NanoDrop 2000c UV-Vis Spectrophotometer before downstream MinION library construction and sequencing.

Enrichment of circular RNAs

Circular RNAs were enriched as described in Figure 1A, using the RPAD method (RNase R treatment, polyadenylation, and poly(A)+RNA depletion) with minor modifications (Panda et al. 2017). Briefly, 100 μg total RNA was dispensed into ten 1.5 mL RNase-free tubes, 10 μg of RNA per tube, followed by incubation with 30U RNase R (per tube) at 37°C for 15 min. After purification, the undigested RNA fragments were mixed with 3U poly (A) polymerase I (AM1350, Thermo Fisher Scientific) to add poly(A) tails *in vitro*. A subsequent removal of poly (A)+RNAs with the Dynabeads™ mRNA Purification Kit and removal of rRNAs with the RiboMinus™ Plant Kit for RNA-Seq (A10838-08, Thermo Fisher Scientific) enriched our preparations with pure circular RNAs for downstream library construction. Primers used in this study are listed in Table S4.

Direct sequencing of circular RNAs using MinION

First, circular RNAs were fragmented using RNA Fragmentation Reagents (AM8740, Ambion), since circular RNAs have a covalent closed-loop, and then collected with the RNA Clean & Concentrator-5 kit (Cat.#R1015, Zymo Research). Subsequently, the fragmented RNAs were dephosphorylated at their 3′ ends with T4 Polynucleotide Kinase (Cat.#M0201V, NEB) and purified with RNA Clean & Concentrator-5 kit (Cat.#R1015, Zymo Research). The RT adapter supplied in the Direct RNA sequencing kit includes an oligo$(dT)_{10}$ primer, designed for poly(A)-tailed RNAs, which will not hybridize to fragmented circular RNAs, since they lack a poly(A) tail. Instead, we attached a customized RT adapter with 10 degenerate primers 'N' (N=A/C/G/T) at the 3′ end to replace the original $(dT)_{10}$. Fragmented circular RNAs attached with sequencing adapter were then sequenced on a MinION platform according to manufacturer's instructions for sequence-specific direct RNA sequencing (SQK-RNA002, Nanopore).

Computational pipeline for detecting circular RNAs and modifications from DRS data

To comprehensively map back-spliced junction reads and annotate circular RNAs containing m^6A modification from DRS with high confidence, all circularized single intron, exon and multiple exons (including internal introns) were multiplied twice to construct a comprehensive virtual sequencing library that would include all potential circular RNAs containing back-splicing junctions. We then removed duplicates from the reads generated from Nanopore sequencer and aligned remaining reads to the virtual circular RNAs sequences using the minimap2 algorithm with default parameters (Li 2016). Candidate transcripts from RNA direct sequencing spanning back-splicing junction sites were retained to further compare them to existing gene annotations in order to obtain the precise positions of donor or acceptor splice sites for each predicted circular RNA. According to the number of exons, exonic circular RNAs (circRNAs) were grouped into distinct subsets to determine whether circularized exons enriched in a specific subset. The average length of distribution of back-spliced exons was independently calculated for circular RNAs with only one circularized exon or multiple exons, respectively. Back-spliced junction regions included in each unique circular RNAs were quantified by RPM (reads per million mapped reads).

The m^6A modification of circular RNAs was detected according to direct RNA sequencing reads using EpiNano tool (Liu et al. 2019) with default parameters. To systematically characterize features of circular RNAs containing the m^6A modification, we performed a number of analyses, which included relative positions between m^6A modification and splice site, the number and length distribution of circularized exons, as well as flanking introns between all detected circRNAs and circRNAs containing m^6A modification. We applied BiNGO (Maere et al. 2005) in Cytoscape for GO enrichment analysis of parental genes resulting in circular RNAs or circular RNAs containing m^6A modification.

Characterization of coding circular RNAs

We used CNCI (https://github.com/www-bioinfo-org/CNCI), CPC (http://cpc.cbi.pku.edu.cn), and Swiss-Port annotation with default parameters to evaluate the coding potential of circular transcripts. Translational enhancing elements such as IRESs of circular transcripts were predicted with the IRESfinder tool, which identifies core IRES regions using framed k-mer features (Zhao et al. 2018b).

Given the possibility that open reading frames (ORFs) translated from circRNAs may span circular junction several times, we first followed a previous method (Pamudurti et al. 2017) and multiplied four times for circRNA sequences, excluding introns, and then predicted ORFs of at least 200 amino acids in length using Transdecoder (Haas et al. 2013). Subsequently, all non-redundant predicted ORFs were mapped to the nr (Non-Redundant) protein sequence database at the National Center for Biotechnology Information (NCBI) using the Basic Local Alignment Tool for Proteins (BLASTP) to detect their homologous proteins with known function using following parameters: score >80, E-value <0.01.

ACKNOWLEDGEMENTS

This work was supported by the National Key Research and Development Program of China (2018YFD0600101), the National Natural Science Foundation of China Grant (Grant No. 31971734), and Program for scientific and technological innovation team in University of Fujian province (No. 118/KLA18069A).

AUTHOR CONTRIBUTIONS

L.F.G. and A.R. conceived and designed the study. Y.S.W., H.Y.W., F.F.X., X.M.H., W.T.W., H.X.Z., and Q.Y.Z. performed the experiments. Y.S.W. and H.Y.W. analyzed high-throughput sequencing data. Y.S.W., H.Y.W., Y.S.Z., Q.Z., M.K., A.R., and L.F.G. analyzed the data as a whole and wrote the manuscript. All authors have read and approved of its content.

COMPETING FINANCIAL INTERESTING

The authors declare no competing financial interests.

DATA AVAILABILITY

Raw Nanopore DRS data has been submitted to the NCBI Gene Expression Omnibus under accession no PRJNA613867. All locus identifiers and circRNAs are available in http://forestry.fafu.edu.cn/pub/circDRS.

REFERENCES

Alarcon CR, Goodarzi H, Lee H, Liu X, Tavazoie S, Tavazoie SF (2015) HNRNPA2B1 is a mediator of m(6)A-dependent nuclear RNA processing events. **Cell** 162: 1299–1308

Arango D, Sturgill D, Alhusaini N, Dillman AA, Sweet TJ, Hanson G, Hosogane M, Sinclair WR, Nanan KK, Mandler MD, Fox SD, Zengeya TT, Andresson T, Meier JL, Coller J, Oberdoerffer S (2018) Acetylation of cytidine in mRNA promotes translation efficiency. **Cell** 175: e1824. 1872-1886

Bailey AS, Batista PJ, Gold RS, Chen YG, de Rooij DG, Chang HY, Fuller MT (2017) The conserved RNA helicase YTHDC2 regulates the transition from proliferation to differentiation in the germline. **eLife** 6: e26116

Bokar JA, Shambaugh ME, Polayes D, Matera AG, Rottman FM (1997) Purification and cDNA cloning of the AdoMet-binding subunit of the human mRNA (N6-adenosine)-methyltransferase. **RNA** 3: 1233–1247

Burd CE, Jeck WR, Liu Y, Sanoff HK, Wang Z, Sharpless NE (2010) Expression of linear and novel circular forms of an INK4/ARF-associated non-coding RNA correlates with atherosclerosis risk. **PLoS Genet** 6: e1001233

Capel B, Swain A, Nicolis S, Hacker A, Walter M, Koopman P, Goodfellow P, Lovell-Badge R (1993) Circular transcripts of the testis-determining gene *Sry* in adult mouse testis. **Cell** 73: 1019–1030

Carlile TM, Rojas-Duran MF, Zinshteyn B, Shin H, Bartoli KM, Gilbert WV (2014) Pseudouridine profiling reveals regulated mRNA pseudouridylation in yeast and human cells. **Nature** 515: 143–146

Chen LL (2016) The biogenesis and emerging roles of circular RNAs. **Nat Rev Mol Cell Biol** 17: 205–211

Chuang TJ, Chen YJ, Chen CY, Mai TL, Wang YD, Yeh CS, Yang MY, Hsiao YT, Chang TH, Kuo TC, Cho HH, Shen CN, Kuo HC, Lu MY, Chen YH, Hsieh SC, Chiang TW (2018) Integrative transcriptome sequencing reveals extensive alternative trans-splicing and cis-backsplicing in human cells. **Nucleic Acids Res** 46: 3671–3691

Cocquerelle C, Daubersies P, Majerus MA, Kerckaert JP, Bailleul B (1992) Splicing with inverted order of exons occurs proximal to large introns. **EMBO J** 11: 1095–1098

Cocquerelle C, Mascrez B, Hetuin D, Bailleul B (1993) Mis-splicing yields circular RNA molecules. **FASEB J** 7: 155–160

Conn VM, Hugouvieux V, Nayak A, Conos SA, Capovilla G, Cildir G, Jourdain A, Tergaonkar V, Schmid M, Zubieta C (2017a) A circRNA from SEPALLATA3 regulates splicing of its cognate mRNA through R-loop formation. **Nat Plants** 3: 17053

Conn VM, Hugouvieux V, Nayak A, Conos SA, Capovilla G, Cildir G, Jourdain A, Tergaonkar V, Schmid M, Zubieta C, Conn SJ (2017b) A circRNA from SEPALLATA3 regulates splicing of its cognate mRNA through R-loop formation. **Nat Plants** 3: 17053

Csepany T, Lin A, Baldick CJ, Jr., Beemon K (1990) Sequence specificity of mRNA N6-adenosine methyltransferase. **J Biol Chem** 265: 20117–20122

Dominissini D, Moshitch-Moshkovitz S, Schwartz S, Salmon-Divon M, Ungar L, Osenberg S, Cesarkas K, Jacob-Hirsch J, Amariglio N, Kupiec M, Sorek R, Rechavi G (2012) Topology of the human and mouse m6A RNA methylomes revealed by m6A-seq. **Nature** 485: 201–206

Dominissini D, Nachtergaele S, Moshitch-Moshkovitz S, Peer E, Kol N, Ben-Haim MS, Dai Q, Di Segni A, Salmon-Divon M, Clark WC, Zheng G, Pan T, Solomon O, Eyal E, Hershkovitz V, Han D, Dore LC, Amariglio N, Rechavi G, He C (2016) The dynamic N(1)-methyladenosine methylome in eukaryotic messenger RNA. **Nature** 530: 441–446

Ebert MS, Neilson JR, Sharp PA (2007) MicroRNA sponges: Competitive inhibitors of small RNAs in mammalian cells. **Nat Methods** 4: 721–726

Edupuganti RR, Geiger S, Lindeboom RGH, Shi H, Hsu PJ, Lu Z, Wang SY, Baltissen MPA, Jansen P, Rossa M, Muller M, Stunnenberg HG, He C, Carell T, Vermeulen M (2017) N (6)-methyladenosine (m(6)A) recruits and repels proteins to regulate mRNA homeostasis. **Nat Struct Mol Biol** 24: 870–878

Franco-Zorrilla JM, Valli A, Todesco M, Mateos I, Puga MI, Rubio-Somoza I, Leyva A, Weigel D, Garcia JA, Paz-Ares J (2007) Target mimicry provides a new mechanism for regulation of microRNA activity. **Nat Genet** 39: 1033–1037

Garalde DR, Snell EA, Jachimowicz D, Sipos B, Lloyd JH, Bruce M, Pantic N, Admassu T, James P, Warland A, Jordan M, Ciccone J, Serra S, Keenan J, Martin S, McNeill L, Wallace EJ, Jayasinghe L, Wright C, Blasco J, Young S, Brocklebank D, Juul S, Clarke J, Heron AJ, Turner DJ (2018) Highly parallel direct RNA sequencing on an array of nanopores. **Nat Methods** 15: 201–206

Garcia-Campos MA, Edelheit S, Toth U, Safra M, Shachar R, Viukov S, Winkler R, Nir R, Lasman L, Brandis A (2019) Deciphering the "m6A Code" via antibody-independent quantitative profiling. **Cell** 178: e716.e16–747.e16

Ge W, Zhang Y, Cheng Z, Hou D, Li X, Gao J (2017) Main regulatory pathways, key genes and microRNAs involved in flower formation and development of moso bamboo (*Phyllostachys edulis*). **Plant Biotechnol J** 15: 82–96

Ghaemmaghami S, Huh WK, Bower K, Howson RW, Belle A, Dephoure N, O'Shea EK, Weissman JS (2003) Global analysis of protein expression in yeast. **Nature** 425: 737–741

Haas BJ, Papanicolaou A, Yassour M, Grabherr M, Blood PD, Bowden J, Couger MB, Eccles D, Li B, Lieber M, MacManes MD, Ott M, Orvis J, Pochet N, Strozzi F, Weeks N, Westerman R, William T, Dewey CN, Henschel R, LeDuc RD, Friedman N, Regev A (2013) De novo transcript sequence reconstruction from RNA-seq using the Trinity platform for reference generation and analysis. **Nat Protoc** 8: 1494–1512

Hansen TB, Jensen TI, Clausen BH, Bramsen JB, Finsen B, Damgaard CK, Kjems J (2013) Natural RNA circles function as efficient microRNA sponges. **Nature** 495: 384–388

Hansen TB, Wiklund ED, Bramsen JB, Villadsen SB, Statham AL, Clark SJ, Kjems J (2011) miRNA-dependent gene silencing involving Ago2-mediated cleavage of a circular antisense RNA. **EMBO J** 30: 4414–4422

Harper JE, Miceli SM, Roberts RJ, Manley JL (1990) Sequence specificity of the human mRNA N6-adenosine methylase *in vitro*. **Nucleic Acids Res** 18: 5735–5741

Holdt LM, Stahringer A, Sass K, Pichler G, Kulak NA, Wilfert W, Kohlmaier A, Herbst A, Northoff BH, Nicolaou A, Gabel G, Beutner F, Scholz M, Thiery J, Musunuru K, Krohn K, Mann M, Teupser D (2016) Circular non-coding RNA ANRIL modulates ribosomal RNA maturation and atherosclerosis in humans. **Nat Commun** 7: 12429

Hsu PJ, Zhu Y, Ma H, Guo Y, Shi X, Liu Y, Qi M, Lu Z, Shi H, Wang J, Cheng Y, Luo G, Dai Q, Liu M, Guo X, Sha J, Shen B, He C (2017) Ythdc2 is an N(6)-methyladenosine binding protein that regulates mammalian spermatogenesis. **Cell Res** 27: 1115–1127

Huang H, Weng H, Sun W, Qin X, Shi H, Wu H, Zhao BS, Mesquita A, Liu C, Yuan CL, Hu YC, Huttelmaier S, Skibbe JR, Su R, Deng X, Dong L, Sun M, Li C, Nachtergaele S, Wang Y, Hu C, Ferchen K, Greis KD, Jiang X, Wei M, Qu L, Guan JL, He C, Yang J, Chen J (2018) Recognition of RNA N(6)-methyladenosine by IGF2BP proteins enhances mRNA stability and translation. **Nat Cell Biol** 20: 285–295

Ivanov A, Memczak S, Wyler E, Torti F, Porath HT, Orejuela MR, Piechotta M, Levanon EY, Landthaler M, Dieterich C, Rajewsky N (2015) Analysis of intron sequences reveals hallmarks of circular RNA biogenesis in animals. **Cell Rep** 10: 170–177

Jain D, Puno MR, Meydan C, Lailler N, Mason CE, Lima CD, Anderson KV, Keeney S (2018) ketu mutant mice uncover an essential meiotic function for the ancient RNA helicase YTHDC2. **eLife** 7: e30919

Jeck WR, Sorrentino JA, Wang K, Slevin MK, Burd CE, Liu J, Marzluff WF, Sharpless NE (2013) Circular RNAs are abundant, conserved, and associated with ALU repeats. **RNA** 19: 141–157

Jia G, Fu Y, Zhao X, Dai Q, Zheng G, Yang Y, Yi C, Lindahl T, Pan T, Yang YG, He C (2011) N6-methyladenosine in nuclear RNA is a major substrate of the obesity-associated FTO. **Nat Chem Biol** 7: 885–887

Ke S, Alemu EA, Mertens C, Gantman EC, Fak JJ, Mele A, Haripal B, Zucker-Scharff I, Moore MJ, Park CY, Vagbo CB, Kussnierczyk A, Klungland A, Darnell JE, Jr., Darnell RB (2015) A majority of m6A residues are in the last exons, allowing the potential for 3′ UTR regulation. **Genes Dev** 29: 2037–2053

Lasda E, Parker R (2014) Circular RNAs: diversity of form and function. **RNA** 20: 1829–1842

Legnini I, Di Timoteo G, Rossi F, Morlando M, Briganti F, Sthandier O, Fatica A, Santini T, Andronache A, Wade M, Laneve P, Rajewsky N, Bozzoni I (2017) Circ-ZNF609 is a circular RNA that can be translated and functions in myogenesis. **Mol Cell** 66: e29–37.e9. 22-37

Li A, Chen YS, Ping XL, Yang X, Xiao W, Yang Y, Sun HY, Zhu Q, Baidya P, Wang X, Bhattarai DP, Zhao YL, Sun BF, Yang YG (2017) Cytoplasmic m(6)A reader YTHDF3 promotes mRNA translation. **Cell Res** 27: 444–447

Li H (2016) Minimap and miniasm: Fast mapping and de novo assembly for noisy long sequences. **Bioinformatics** 32: 2103–2110

Li L, Hu T, Li X, Mu S, Cheng Z, Ge W, Gao J (2016a) Genome-wide analysis of shoot growth-associated alternative splicing in moso bamboo. **Mol Genet Genomics** 291: 1695–1714

Li S, Mason CE (2014) The pivotal regulatory landscape of RNA modifications. **Annu Rev Genomics Hum Genet** 15: 127–150

Li Z, Huang C, Bao C, Chen L, Lin M, Wang X, Zhong G, Yu B, Hu W, Dai L, Zhu P, Chang Z, Wu Q, Zhao Y, Jia Y, Xu P, Liu H, Shan G (2015) Exon-intron circular RNAs regulate transcription in the nucleus. **Nat Struct Mol Biol** 22: 256–264

Li Z, Wang S, Cheng J, Su C, Zhong S, Liu Q, Fang Y, Yu Y, Lv H, Zheng Y, Zheng B (2016b) Intron lariat RNA inhibits microRNA biogenesis by sequestering the dicing complex in *Arabidopsis*. **PLoS Genet** 12: e1006422

Liang D, Tatomer DC, Luo Z, Wu H, Yang L, Chen LL, Cherry S, Wilusz JE (2017) The output of protein-coding genes shifts to circular RNAs when the pre-mRNA processing machinery is limiting. **Mol Cell** 68: e943.e3–954.e3

Liu H, Begik O, Lucas MC, Ramirez JM, Mason CE, Wiener D, Schwartz S, Mattick JS, Smith MA, Novoa EM (2019) Accurate detection of m(6)A RNA modifications in native RNA sequences. **Nat Commun** 10: 4079

Liu J, Yue Y, Han D, Wang X, Fu Y, Zhang L, Jia G, Yu M, Lu Z, Deng X, Dai Q, Chen W, He C (2014) A METTL3-METTL14 complex mediates mammalian nuclear RNA N6-adenosine methylation. **Nat Chem Biol** 10: 93–95

Liu N, Dai Q, Zheng G, He C, Parisien M, Pan T (2015) N(6)-methyladenosine-dependent RNA structural switches regulate RNA-protein interactions. **Nature** 518: 560–564

Liu N, Zhou KI, Parisien M, Dai Q, Diatchenko L, Pan T (2017) N6-methyladenosine alters RNA structure to regulate binding of a low-complexity protein. **Nucleic Acids Res** 45: 6051–6063

Liu Y, Deng Y, Li G, Zhao J (2013) Replication factor C1 (RFC1) is required for double-strand break repair during meiotic homologous recombination in *Arabidopsis*. **Plant J** 73: 154–165

Maere S, Heymans K, Kuiper M (2005) BiNGO: A Cytoscape plugin to assess overrepresentation of gene ontology categories in biological networks. **Bioinformatics** 21: 3448–3449

Memczak S, Jens M, Elefsinioti A, Torti F, Krueger J, Rybak A, Maier L, Mackowiak SD, Gregersen LH, Munschauer M, Loewer A, Ziebold U, Landthaler M, Kocks C, le Noble F, Rajewsky N (2013) Circular RNAs are a large class of animal RNAs with regulatory potency. **Nature** 495: 333–338

Meyer KD, Jaffrey SR (2014) The dynamic epitranscriptome: N6-methyladenosine and gene expression control. **Nat Rev Mol Cell Biol** 15: 313–326

Meyer KD, Saletore Y, Zumbo P, Elemento O, Mason CE, Jaffrey SR (2012) Comprehensive analysis of mRNA methylation reveals enrichment in 3′ UTRs and near stop codons. **Cell** 149: 1635–1646

Molinie B, Wang J, Lim KS, Hillebrand R, Lu ZX, Van Wittenberghe N, Howard BD, Daneshvar K, Mullen AC, Dedon P, Xing Y, Giallourakis CC (2016) m(6)A-LAIC-seq reveals the census and complexity of the m(6)A epitranscriptome. **Nat Methods** 13: 692–698

Nigro JM, Cho KR, Fearon ER, Kern SE, Ruppert JM, Oliner JD, Kinzler KW, Vogelstein B (1991) Scrambled exons. **Cell** 64: 607–613

Pamudurti NR, Bartok O, Jens M, Ashwal-Fluss R, Stottmeister C, Ruhe L, Hanan M, Wyler E, Perez-Hernandez D, Ramberger E, Shenzis S, Samson M, Dittmar G, Landthaler M, Chekulaeva M, Rajewsky N, Kadener S (2017) Translation of CircRNAs. **Mol Cell** 66: e27–21.e7

Panda AC, De S, Grammatikakis I, Munk R, Yang X, Piao Y, Dudekula DB, Abdelmohsen K, Gorospe M (2017) High-purity circular RNA isolation method (RPAD) reveals vast collection of intronic circRNAs. **Nucleic Acids Res** 45: e116

Parker MT, Knop K, Sherwood AV, Schurch NJ, Mackinnon K, Gould PD, Hall AJ, Barton GJ, Simpson GG (2020) Nanopore direct RNA sequencing maps the complexity of *Arabidopsis* mRNA processing and m(6)A modification. **eLife** 9

Pasman Z, Been MD, Garcia-Blanco MA (1996) Exon circularization in mammalian nuclear extracts. **RNA** 2: 603–610

Peng Z, Lu Y, Li L, Zhao Q, Feng Q, Gao Z, Lu H, Hu T, Yao N, Liu K, Li Y, Fan D, Guo Y, Li W, Lu Y, Weng Q, Zhou C, Zhang L, Huang T, Zhao Y, Zhu C, Liu X, Yang X, Wang T, Miao K, Zhuang C, Cao X, Tang W, Liu G, Liu Y, Chen J, Liu Z, Yuan L, Liu Z, Huang X, Lu T, Fei B, Ning Z, Han B, Jiang Z (2013) The draft genome of the fast-growing non-timber forest species moso bamboo (*Phyllostachys heterocycla*). **Nat Genet** 45: e451–e452. 456-461

Ping XL, Sun BF, Wang L, Xiao W, Yang X, Wang WJ, Adhikari S, Shi Y, Lv Y, Chen YS, Zhao X, Li A, Yang Y, Dahal U, Lou XM, Liu X, Huang J, Yuan WP, Zhu XF, Cheng T, Zhao YL, Wang X, Rendtlew Danielsen JM, Liu F, Yang YG (2014) Mammalian WTAP is a regulatory subunit of the RNA N6-methyladenosine methyltransferase. **Cell Res** 24: 177–189

Poliseno L, Salmena L, Zhang J, Carver B, Haveman WJ, Pandolfi PP (2010) A coding-independent function of gene and pseudogene mRNAs regulates tumour biology. **Nature** 465: 1033–1038

Roundtree IA, Luo GZ, Zhang Z, Wang X, Zhou T, Cui Y, Sha J, Huang X, Guerrero L, Xie P, He E, Shen B, He C (2017) YTHDC1 mediates nuclear export of N(6)-methyladenosine methylated mRNAs. **eLife** 6: e31311

Salzman J, Chen RE, Olsen MN, Wang PL, Brown PO (2013) Cell-type specific features of circular RNA expression. **PLoS Genet** 9: e1003777

Schwartz S, Bernstein DA, Mumbach MR, Jovanovic M, Herbst RH, Leon-Ricardo BX, Engreitz JM, Guttman M, Satija R, Lander ES, Fink G, Regev A (2014) Transcriptome-wide

mapping reveals widespread dynamic-regulated pseudouridylation of ncRNA and mRNA. **Cell** 159: 148–162

Shi H, Wang X, Lu Z, Zhao BS, Ma H, Hsu PJ, Liu C, He C (2017) YTHDF3 facilitates translation and decay of N(6)-methyladenosine-modified RNA. **Cell Res** 27: 315–328

Shou Y, Zhu Y, Ding Y (2020) Transcriptome analysis of lateral buds from Phyllostachys edulis rhizome during germination and early shoot stages. **BMC Plant Biol** 20: 229

Soneson C, Yao Y, Bratus-Neuenschwander A, Patrignani A, Robinson MD, Hussain S (2019) A comprehensive examination of Nanopore native RNA sequencing for characterization of complex transcriptomes. **Nat Commun** 10: 3359

Tang C, Xie Y, Yu T, Liu N, Wang Z, Woolsey RJ, Tang Y, Zhang X, Qin W, Zhang Y, Song G, Zheng W, Wang J, Chen W, Wei X, Xie Z, Klukovich R, Zheng H, Quilici DR, Yan W (2020) m(6)A-dependent biogenesis of circular RNAs in male germ cells. **Cell Res** 30: 211–228

Templeton GW, Nimick M, Morrice N, Campbell D, Goudreault M, Gingras AC, Takemiya A, Shimazaki K, Moorhead GB (2011) Identification and characterization of AtI-2, an Arabidopsis homologue of an ancient protein phosphatase 1 (PP1) regulatory subunit. **Biochem J** 435: 73–83

Wang PL, Bao Y, Yee MC, Barrett SP, Hogan GJ, Olsen MN, Dinneny JR, Brown PO, Salzman J (2014a) Circular RNA is expressed across the eukaryotic tree of life. **PLoS One** 9: e90859

Wang X, Zhao BS, Roundtree IA, Lu Z, Han D, Ma H, Weng X, Chen K, Shi H, He C (2015) N(6)-methyladenosine modulates messenger RNA translation efficiency. **Cell** 161: 1388–1399

Wang Y, Gao Y, Zhang H, Wang H, Liu X, Xu X, Zhang Z, Kohnen MV, Hu K, Wang H, Xi F, Zhao L, Lin C, Gu L (2019) Genome-wide profiling of circular RNAs in the rapidly growing shoots of moso bamboo (*Phyllostachys edulis*). **Plant Cell Physiol** 60: 1354–1373

Wang Y, Li Y, Toth JI, Petroski MD, Zhang Z, Zhao JC (2014b) N6-methyladenosine modification destabilizes developmental regulators in embryonic stem cells. **Nat Cell Biol** 16: 191–198

Wei CM, Gershowitz A, Moss B (1975) Methylated nucleotides block 5′ terminus of HeLa cell messenger RNA. **Cell** 4: 379–386

Westholm JO, Miura P, Olson S, Shenker S, Joseph B, Sanfilippo P, Celniker SE, Graveley BR, Lai EC (2014) Genome-wide analysis of drosophila circular RNAs reveals their structural and sequence properties and age-dependent neural accumulation. **Cell Rep** 9: 1966–1980

Wilusz JE (2018) A 360 degrees view of circular RNAs: From biogenesis to functions. **Wiley Interdiscip Rev: RNA** 9: e1478

Wojtas MN, Pandey RR, Mendel M, Homolka D, Sachidanandam R, Pillai RS (2017) Regulation of m(6)A transcripts by the 3′-->5′ RNA helicase YTHDC2 is essential for a successful meiotic program in the mammalian germline. **Mol Cell** 68: e312–e387. 374-387

Wu B, Su S, Patil DP, Liu H, Gan J, Jaffrey SR, Ma J (2018) Molecular basis for the specific and multivariant recognitions of RNA substrates by human hnRNP A2/B1. **Nat Commun** 9: 420

Yang Y, Fan X, Mao M, Song X, Wu P, Zhang Y, Jin Y, Yang Y, Chen LL, Wang Y, Wong CC, Xiao X, Wang Z (2017) Extensive translation of circular RNAs driven by N(6)-methyladenosine. **Cell Res** 27: 626–641

Yang Y, Gao X, Zhang M, Yan S, Sun C, Xiao F, Huang N, Yang X, Zhao K, Zhou H, Huang S, Xie B, Zhang N (2018) Novel role of FBXW7 circular RNA in repressing glioma tumorigenesis. **J Natl Cancer Inst** 110: 110–315

Yue Y, Liu J, He C (2015) RNA N6-methyladenosine methylation in post-transcriptional gene expression regulation. **Genes Dev** 29: 1343–1355

Zhang F, Kang Y, Wang M, Li Y, Xu T, Yang W, Song H, Wu H, Shu Q, Jin P (2018a) Fragile X mental retardation protein modulates the stability of its m6A-marked messenger RNA targets. **Hum Mol Genet** 27: 3936–3950

Zhang HX, Wang HH, Zhu Q, Gao YB, Wang HY, Zhao LZ, Wang YS, Xi FH, Wang WF, Yang YQ, Lin CT, Gu LF (2018b) Transcriptome characterization of moso bamboo (Phyllostachys edulis) seedlings in response to exogenous gibberellin applications. **BMC Plant Biol** 18: 125

Zhang P, Fan Y, Sun X, Chen L, Terzaghi W, Bucher E, Li L, Dai M (2019a) A large-scale circular RNA profiling reveals universal molecular mechanisms responsive to drought stress in maize and *Arabidopsis*. **Plant J** 98: 697–713

Zhang XO, Wang HB, Zhang Y, Lu XH, Chen LL, Yang L (2014) Complementary sequence-mediated exon circularization. **Cell** 159: 134–147

Zhang Y, Zhang XO, Chen T, Xiang JF, Yin QF, Xing YH, Zhu S, Yang L, Chen LL (2013) Circular intronic long noncoding RNAs. **Mol Cell** 51: 792–806

Zhang Z, Chen LQ, Zhao YL, Yang CG, Roundtree IA, Zhang Z, Ren J, Xie W, He C, Luo GZ (2019b) Single-base mapping of m6A by an antibody-independent method. **Sci Adv** 5: eaax0250

Zhao H, Gao Z, Wang L, Wang J, Wang S, Fei B, Chen C, Shi C, Liu X, Zhang H, Lou Y, Chen L, Sun H, Zhou X, Wang S, Zhang C, Xu H, Li L, Yang Y, Wei Y, Yang W, Gao Q, Yang H, Zhao S, Jiang Z (2018a) Chromosome-level reference genome and alternative splicing atlas of moso bamboo (*Phyllostachys edulis*). **Gigascience** 7, https://doi.org/10.1093/gigascience/giy115

Zhao J, Wu J, Xu T, Yang Q, He J, Song X (2018b) IRESfinder: Identifying RNA internal ribosome entry site in eukaryotic cell using framed k-mer features. **J Genet Genomics** 45: 403–406

Zheng G, Dahl JA, Niu Y, Fedorcsak P, Huang CM, Li CJ, Vagbo CB, Shi Y, Wang WL, Song SH, Lu Z, Bosmans RP, Dai Q, Hao YJ, Yang X, Zhao WM, Tong WM, Wang XJ, Bogdan F, Furu K, Fu Y, Jia G, Zhao X, Liu J, Krokan HE, Klungland A, Yang YG, He C (2013) ALKBH5 is a mammalian RNA demethylase that impacts RNA metabolism and mouse fertility. **Mol Cell** 49: 18–29

SUPPORTING INFORMATION

Additional Supporting Information may be found online in the supporting information tab for this article: http://onlinelibrary.wiley.com/doi/10.1111/jipb.13002/suppinfo

Table S1. List of all circRNAs based on Nanopore direct RNA sequencing

Table S2. List of circRNAs containing m^6A modification

Table S3. List of circRNAs with continuous ORF

Table S4. Primers used for validation of circular and linear transcripts